Materials Advances

Check for updates

Monodisperse and size-modulable spherical optical resonators produced from synthetic polymers by inkjet printing toward applications under water†

Kariana Kusuma Dewi, [a] Hiroshi Yamagishi, *[a] Wey Yih Heah, [a] Sooyeon Kim, [b] Asuma Kubono, [b] Yuichi Taniguchi [b] and Yohei Yamamoto *[a]

Micro-spherical optical resonators with high monodispersity and size-modulability are produced from synthetic polymers using an inkjet printing method. The high surface smoothness and sphericity of the synthetic polymer particles contribute to the efficient light confinement inside the particles *via* whispering gallery mode (WGM) optical resonance in water, demonstrating their suitability for chemical and biological applications.

In addition to their traditional usage in biological and flow cytometry applications,[1,2] spherical polymer particles have recently gained renewed attention in the field of optics. Optical resonance, particularly whispering gallery mode (WGM) optical resonance, refers to a light confinement phenomenon within a spherical object through iterative total internal reflection along the circumference.[3,4] A distinct outcome of WGM resonance is the appearance of periodic sharp peaks in absorption, transmission, and emission spectra. These peaks are distinguishable with a precision less than one nanometre and serve as highly multiplexed optical barcodes and cell tags.[5–7] In addition, these peaks exhibit spectral shift in response to the changes in the surrounding media, enabling highly precise physical and chemical sensing.[8] Many studies have discussed the potential of spherical geometry as a microresonator and sensor[9,10] with an ultralow-lasing threshold.[11,12]

Spherical particles with uniform morphology and size monodispersity are the fundamental basis for enhancing the sensitivity, precision, and reproducibility of the resonators' performance.[13] Ideally, highly spherical particles with a size modulability less than 1 μm are preferable for generating consistent peaks. Suspension polymerization has been an authentic method for making such particles. The precursor micelles encapsulating monomers and initiators are dispersed in an immiscible liquid and are polymerized therein, yielding spherical particles.[14,15] Polystyrene (PS) beads are the most common product of suspension polymerization, characterized by their highly spherical and monodisperse morphology with a typical polydispersity index (PDI) of 0.1 according to previous reports.[16,17]

Nonetheless, suspension polymerization is still unsatisfactory for making optical resonators regarding the scope of applicable materials. Most of the reports on the synthesis of spherical polymer particles did not disclose their optical performances. In addition, due to the existence of water or other polar solvents in the suspension, several types of polymers are unavailable by suspension polymerization. Over the past few decades, several research groups, including the authors' group, have focused on this topic and tried expanding the scope of applicable materials. For instance, our group has investigated the self-assembly process of polymers in the solution state and discovered that slow precipitation produces microparticles with high sphericity and surface smoothness that are suitable for WGM resonance.[18,19] We also found that this method is widely applicable to organic materials such as organic semiconductors,[20] dendrimers,[21] and porous polymers for membranes.[22] Biological polymers including peptides and polysaccharides are also applicable.[23,24] These new materials are highly promising for the emerging field of laser-based bio-sensing because the resonators and lasers can be biocompatible and chemically tailored, which are unfeasible with the traditional semiconductor lasers.[25] However, this method is still under development, particularly with respect to size modulability and monodispersity. The average PDI of the spherical particles produced by the self-assembly method has often exceeded 0.3, which is inadequate for reproducible and consistent optical measurements.[18]

In this study, we focus on the inkjet printing method. While inkjet printing has gained attention in the field of optics and has already been applied to the formation of resonators, it is

[a] *Department of Material Science, Institute of Pure and Applied Science, University of Tsukuba, 1-1-1 Tennodai, Tsukuba, Ibaraki, 305-8573, Japan. E-mail: yamagishi.hiroshi.ff@u.tsukuba.ac.jp, yamamoto@ims.tsukuba.ac.jp*

[b] *Institute for Integrated Cell-Material Sciences (iCeMS), Kyoto University, Yoshida-Honmachi, Sakyo-ku, Kyoto, 606-8501, Japan*

† Electronic supplementary information (ESI) available. See DOI: https://doi.org/10.1039/d5ma00176e
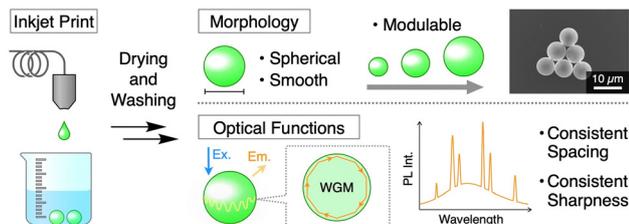
Fig. 1 Schematic illustration of the inkjet printing method for the fabrication of spherical polymer particles with monodisperse and modulable size distribution. The particles exhibit whispering gallery mode (WGM) optical resonance and periodic sharp peaks in the emission spectrum.

limited to the formation of disks and distorted spheres due to the difficulty in maintaining their sphericity and smoothness during the solidification process.[26–28] Our group has also been tackling this topic, but the applicable materials scope of our previous inkjet method was considerably limited and unable to make spheres from synthetic materials.[23] Here, we overcome these difficulties and succeed in making monodisperse spherical optical resonators from synthetic polymers (Fig. 1). Polystyrene, as an authentic example, was dissolved in 1,2-dichloroethane ($C_2H_4Cl_2$) and was injected into water as tiny droplets. In one day, the droplets were solidified and yielded monodisperse spherical particles with a polydispersity index (PDI) of 0.02. The mean of the particle diameter (D) was modulable in a range from 5.4 to 14.1 μm with a precision of 0.5 μm by changing the concentration. This method was applicable to a series of synthetic polymers including polyvinylcarbazole (PVK) and polymethyl methacrylate (PMMA). The excellent sphericity and surface smoothness of the microparticles lead to efficient WGM optical resonance with a peak sharpness as narrow as 1.1 nm although the peaks are not as sharp as typical WGM resonators plausibly due to the reabsorption of the dyes and the absence of the tapered optical setup.[29] The WGM peaks were observed even under water, demonstrating their potential for the biological optical probing in the future.

We used an inkjet printing machine specialized for viscous liquid (Microjet model LaboJet-600). As a typical example, an aliquot of $C_2H_4Cl_2$ solution of PS (1.0 mg mL^{-1}) doped with 9,10-bis(phenylethynyl)anthracene (BPEA, 5.0 μg mL^{-1}) was introduced into the inkjet printer head and was ejected as tiny drops with a D of 72.5 μm (Fig. S1a, ESI†). The droplets were produced consecutively with a repetition rate of 120 Hz for 30 min and were injected onto a PTFE dish containing a 5 mL aqueous solution of polyvinyl alcohol (PVA, 0.5 wt%). The deposited droplets went into the water and sank to the bottom of the dish because of the large density of $C_2H_4Cl_2$. The droplets (Fig. S1b, ESI†) sitting on the bottom of the dish were spherical without adhering to the dish due to the oleophobicity of PTFE. The droplets eventually solidified in water without coalescence after incubation at 25 °C for 1 day without capping (Fig. S1c, ESI†). The resulting precipitates were washed with water three times and were observed with an optical microscope (OM), a fluorescence microscope (FM), and a scanning electron microscope (SEM).
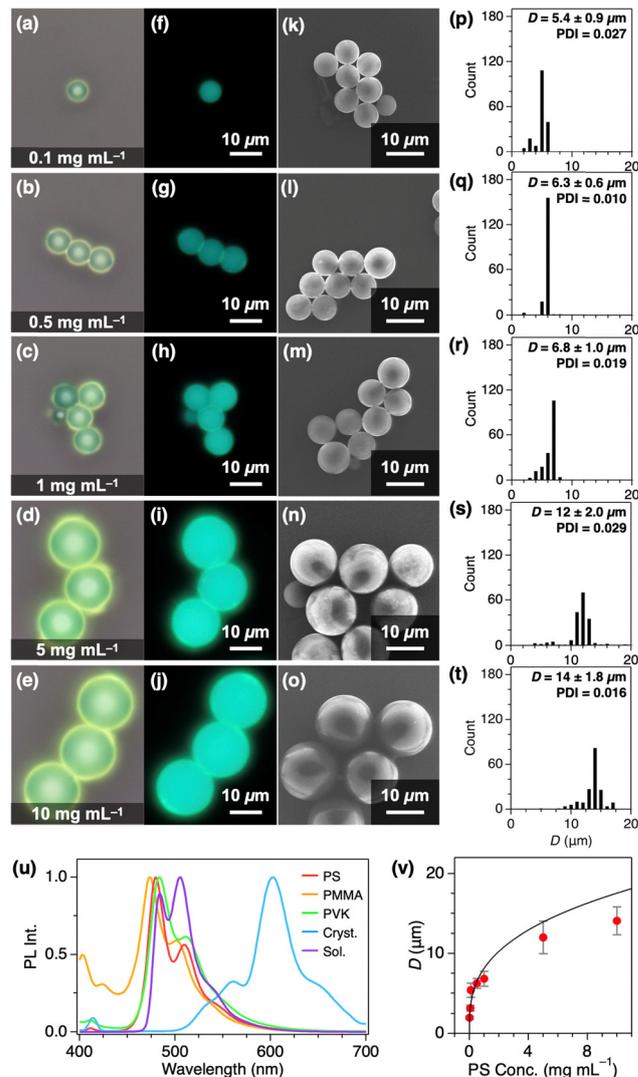
Fig. 2 Optical microscopy (a)–(e), fluorescence microscopy (f)–(j), (λ_{ex} = 400–440 nm), SEM images (k)–(o), and histograms of D (p)–(t), (n = 179) of PS microspheres produced using solutions with different concentrations (0.1, 0.5, 1.0, 5.0, and 10 mg mL^{-1}). (u) PL spectra (λ_{ex} = 365 nm) of BPEA (0.5 wt%) doped in PS (red curve), PMMA (orange curve), PVK (green curve) films together with BPEA in the crystalline state (blue curve) and in the solution state ($C_2H_4Cl_2$, 0.05 mg mL^{-1}, purple curve). (v) A plot of average D of PS microspheres against the concentration used for the inkjet printing. The black curve represents the theoretical values. Error bars represent the standard deviations.

SEM images revealed the spherical morphology and the smooth surface of the precipitates with an average D of 6.83 μm and a standard deviation (σ) of 0.95 μm (Fig. 2m). The smoothness of the surface was quantitatively evaluated based on the root-mean-square (RMS) roughness value. The values are consistently low regardless of the concentration utilized (Fig. S2, ESI†). The spherical morphology was also evident in the OM and FM images (Fig. 2c and h). As a comparison, we conducted the same inkjet procedure by using different good organic solvents as summarized in Fig. S2 (ESI†), but they were less successful. Precipitates obtained from 1,

2-diclorobenzene and chlorobenzene solutions of PS were not smooth, which is disadvantageous for optical resonance. When $CHCl_3$, toluene and N,N-dimethylformamide (DMF) were utilized as the solvents instead of $C_2H_4Cl_2$, the quantity of the collected precipitates was considerably small, and their surface smoothness was not as good as those obtained from $C_2H_4Cl_2$ judging from the RMS values (Fig. S2, ESI†). Small yield is plausibly due to the floating of the droplets at the water surface, leading to the accumulation and adhesion of the droplets at the periphery of the dish.

The inkjet method was feasible to make spheres with different concentrations of PS in a range from 0.1 to 10 mg mL^{-1}. The microscopic images of the resulting precipitates for each concentration showed consistent spherical morphology with a smooth surface (Fig. 2a–o), while the average D increased upon condensing the solution (Fig. 2p–t). The available range of D was from 5.4 to 14.1 μm, maintaining satisfactory σ and PDI (Table S1, ESI†). The plot of D against the concentration follows the theoretical curve. In theory, D should follow a cubic root function of the polymer concentration given that the volume of the droplet was consistent regardless of the concentration (Fig. 2v). The theoretical curve essentially traces the experimentally observed diameters, while the deviations become pronounced at higher concentration plausibly because of the higher viscosity of the concentrated solution and associated change in the size of the droplets.[30] Notably, the experimentally demonstrated modulability of D was less than 1 μm (0.5 μm). Likewise, as a demonstration of the feasibility of the inkjet method, we replaced BPEA with Nile Red and pyrromethene and conducted the same procedure. As expected, the resulting particles showed sharp peaks in μ-PL spectra (Fig. S3, ESI†).

We measured the micro-photoluminescence (μ-PL) spectra from individual particles using a custom-built light-sheet microscope equipped with an excitation laser (λ_{ex} = 488 nm), imaging spectrometer, and EM-CCD camera.[31] The aqueous suspension of the polymer particles was drop-cast onto a transparent film substrate and was then air-dried. The excitation laser was focused through an illumination objective lens and scanned over the entire view with a scanning rate of 1.07 kHz. The laser passed through the film and excited the microparticles, inducing photoluminescence (PL) of the BPEA dyes inside the particles. The emission from a single particle was collected through the detection objective lens, transferred to the spectrometer and imaged with an EM-CCD camera.

While the typical PL spectrum from BPEA in the film state (λ_{ex} = 365 nm) featured a broad spontaneous emission band centred at 480 nm (Fig. 2u), the μ-PL spectrum of the PS microspheres doped with BPEA showed periodic sharp peaks overlapping the spontaneous emission band (Fig. 3a–c). The peaks were assignable to the series of transverse electric (TE) and magnetic (TM) modes of WGM according to the theoretical equations[32] and were indexed accordingly (Fig. S4, ESI†). The shoulder band at 550 nm appeared to be more prominent at higher concentrations, which is plausibly because of the enhanced reabsorption by the concentrated dyes.[33] WGM is further supported by the plot of the free spectral range (FSR)
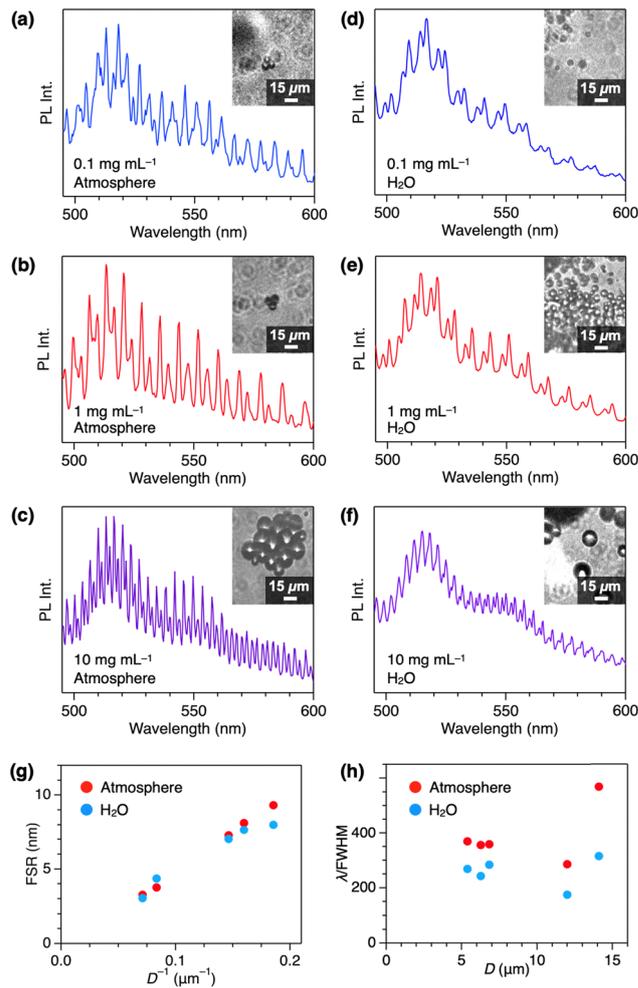
Fig. 3 μ-PL spectra (λ_{ex} = 488 nm) of PS microspheres produced from solutions with concentrations of 0.1 (a) and (d), 1 (b) and (e), and 10 mg mL^{-1} (c) and (f). The spectra were taken under the atmosphere (a)–(c) and under water (d)–(f). The insets show the microscopic images of the PS microspheres subjected to the μ-PL measurements. Scale bars represent 15 μm. (g) Average FSR of PS microspheres observed under the atmosphere (red circles) and under water (blue circles) plotted against the inverse of D. (h) λ/FWHM of PS microspheres observed under the atmosphere (red circles) and under water (blue circles) plotted against D.

against the inverse of the diameter (D^{-1}) of the spheres, displaying a linear correlation as expected from the theory (Fig. 3g). Noteworthily, the distribution of the FSR was also monodispersed with the minimum σ of 0.21 nm (Table S2, ESI†), which is a valuable consequence of the size-monodispersity of the spheres. The slightly smaller FSR under water is due to the higher refractive index of water in comparison to the air.[34] Likewise, λ/FWHM values of the spheres, quantitative values representing the efficiency of the light confinement, were nearly equal to each other (Fig. 3h), while the λ/FWHM values of the largest microparticles were relatively higher than the others likely due to the better sphericity. The peak broadening under water is likely due to the enhanced light leakage, which is caused by the small difference in the refractive index between the polymer matrix and the surrounding medium.[35]
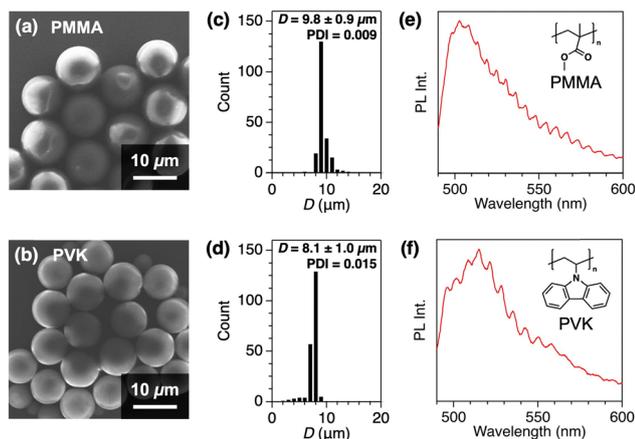
Fig. 4 Scanning electron micrographs (a) and (b), histograms of D (n = 205) (c) and (d), and microscopic photoluminescence spectra (μ-PL, λ_{ex} = 450 nm) (e) and (f) of polymethyl methacrylate (PMMA), (a), (c) and (e) and polyvinylcarbazole (PVK), (b), (d) and (f) microspheres produced from $C_2H_4Cl_2$ solutions (2 mg mL^{-1}) through the inkjet printing method.

The inkjet method was applicable to PMMA and PVK as well, demonstrating the broad applicability of the method particularly to synthetic polymers. We conducted the same inkjet procedure as that for PS by dissolving each polymer with $C_2H_4Cl_2$ with a concentration of 2 mg mL^{-1}. The resulting polymer particles produced from PMMA and PVK were both highly spherical and smooth with PDIs of 0.0093 and 0.0155, respectively (Fig. 4a–d). The size modulability was also demonstrated with PMMA and PVK by using solutions with three different concentrations (0.5, 1.0, and 2.0 mg mL^{-1}, Fig. 4 and Fig. S5, ESI†). The size distribution of PVK spheres was relatively broader than that of PS and PMMA because of the unstable ejection of the droplets. Nonetheless, all the spheres were eligible for the optical resonance and exhibited sharp periodic peaks as shown in their μ-PL spectra (λ_{ex} = 450 nm, Fig. 4e and f, see ESI† for the details of the μ-PL measurements). The emission band of PMMA microspheres in the μ-PL spectra is located at a slightly blue-shifted region in comparison to that of PS and PVK, which is consistent with the PL spectra in the film state (Fig. 2u). Note that the emission bands of BPEA were significantly blue-shifted in comparison to that of the crystalline state of BPEA (Fig. 2u). This is because the BPEA dyes were dispersed at a molecular level in the film. Consistently, the emission band of BPEA in the solution state ($C_2H_4Cl_2$) was analogous to that in the film state (Fig. 2u). We also examined the optical stability of the spheres. Upon continuous excitation, the PL intensities gradually decreased within 10 min (Fig. S6, ESI†), which was satisfactory for us to conduct the optical measurements with high reproducibility.

We also conducted μ-PL measurements under water. The suspension of the spheres was drop-cast onto a film substrate and air-dried, onto which an aliquot of deionized water (100 μL) was mounted to fully cover the spheres. The film was set on the μ-PL and was subjected to the measurements. The μ-PL spectra obtained under water (Fig. 3d–f) were essentially analogous to

those observed under the atmosphere. The WGM peaks were analogous for all spheres tested (PS microspheres produced from solutions with concentrations of 0.1, 0.5, 1.0, 5.0, and 10 mg mL^{-1}) particularly in terms of the FSR values (Fig. 3g and Fig. S7, ESI†) although their λ/FWHM was slightly lower than those under the atmosphere (Fig. 3h and Table S3, ESI†). The attenuation of λ/FWHM is reasonable based on the theory claiming that λ/FWHM is correlated with the refractive index of the surrounding medium as well as the sphere itself.[35] λ/FWHM usually decreases upon increasing the refractive index of the surrounding medium, which corresponds to the underwater measurements. The fact that the WGM peaks were still visible even under water is a promising finding since it demonstrates the versatility of the inkjet method for making optical resonators that are functional under biological conditions. The analogous sharp peaks were also observable even when using aqueous PBS solution containing BSA (0.1 wt%, Fig. S8, ESI†). As an additional demonstration, we also tried to observe stimulated emission, but it was not observed (Fig. S9, ESI†).

In conclusion, monodisperse PS microspheres have been successfully fabricated using an inkjet printing method. A suitable solution of polymers can be injected into water to form stable droplets, which eventually solidified to form spherical particles. The available diameter of the spheres ranged from 5.4 to 14.1 μm with a minimum precision of 0.5 μm depending on the concentration of the polymer solution. The diameter of the spheres was highly monodispersed with a PDI as small as 0.009. The photoluminescent microspheres exhibited sharp peaks due to the optical resonance inside of the sphere. As a consequence of the uniform size, these spheres show a consistent free spectral range and λ/FWHM, which are valuable for reproducible optical measurements. The spheres exhibited resonance peaks even under water, demonstrating their potential value for the future applications in biological sensing.

Data availability

The data supporting this article have been included as part of the ESI.†

Conflicts of interest

There are no conflicts to declare.

Acknowledgements

References

1 T. Kishida, *Adv. Mater. Interfaces*, 2024, **11**, 2301028.

2 B. J. Battersby, G. A. Lawrie and M. Trau, *Drug Discovery Today*, 2001, **6**, S19–S26.

3 S. Yang, Y. Wang and H. Sun, *Adv. Opt. Mater.*, 2015, **3**, 1136–1162.

4 A. Chiasera, Y. Dumeige, P. Féron, M. Ferrari, Y. Jestin, G. Nunzi Conti, S. Pelli, S. Soria and G. C. Righini, *Laser Photon. Rev.*, 2010, **4**, 457–482.

5 D. Richter, M. Marincic and M. Humar, *Lab Chip*, 2020, **20**, 734–740.

6 A. R. Anwar, M. Mur and M. Humar, *ACS Photonics*, 2023, **10**, 1202–1224.

7 J. Liao and L. Yang, *Light: Sci. Appl.*, 2021, **10**, 32.

8 I. Brice, K. Grundsteins, K. Draguns, A. Atvars and J. Alnis, *Sensors*, 2021, **21**, 7184.

9 W. Du, S. Zhang, Z. Wu, Q. Shang, Y. Mi, J. Chen, C. Qin, X. Qiu, Q. Zhang and X. Liu, *Nanoscale*, 2019, **11**, 3138–3144.

10 X. Wang, C. Huang, C. Xia, F. Qin, G. Zhu, L. Mao, Y. Ma, Z. Shi, Q. Cui and C. Xu, *Sci Bull.*, 2024, **69**, 2021–2024.

11 R. Duan, Z. Zhang, L. Xiao, X. Zhao, Y. T. Thung, L. Ding, Z. Liu, J. Yang, V. D. Ta and H. Sun, *Adv. Mater.*, 2022, **34**, 2108884.

12 X. Wang, Z. Li, R. Wang, G. Zhu, F. Qin, J. Chen, J. Wang, Z. Shi, Q. Cui and C. Xu, *Appl. Phys. Lett.*, 2021, **119**, 021101.

13 T. V. Nguyen, T. D. Nguyen, N. V. Pham, T. A. Nguyen and D. V. Ta, *Opt. Lett.*, 2021, **46**, 2517–2520.

14 L. Duan, J. Fan, G. Chen, P. Qiu, X. Zhang and X. Zhai, *Colloids Surf., A*, 2025, **709**, 136125.

15 A. Xu, Y. Sun and M. Guo, *Macromol. Biosci.*, 2024, **24**, e2400047.

16 P. Sálek and D. Horák, *E-Polymers*, 2011, **11**, 064.

17 Z. Dastbaz, S. N. Dana and S. N. Ashrafizadeh, *RSC Adv.*, 2021, **11**, 17547–17557.

18 S. Nakayama, H. Yamagishi, O. Oki, S. Kushida, J. Chen, J. Kuwabara, T. Kanbara, W. Yospanya, R. Oda and Y. Yamamoto, *Chem. Commun.*, 2024, **60**, 7634–7637.

19 Suharman, W. Y. Heah, H. Yamagishi and Y. Yamamoto, *Nanoscale*, 2023, **15**, 19062–19068.

20 O. Oki, C. Kulkarni, H. Yamagishi, S. C. J. Meskers, Z.-H. Lin, J.-S. Huang, E. W. Meijer and Y. Yamamoto, *J. Am. Chem. Soc.*, 2021, **143**, 8772–8779.

21 K. Iwai, H. Yamagishi, C. Herzberger, Y. Sato, H. Tsuji, K. Albrecht, K. Yamamoto, F. Sasaki, H. Sato, A. Asaithambi, A. Lorke and Y. Yamamoto, *Angew. Chem., Int. Ed.*, 2020, **59**, 12674–12679.

22 N. Tanji, H. Yamagishi, K. Fujita and Y. Yamamoto, *ACS Appl. Polym. Mater.*, 2022, **4**, 1065–1070.

23 W. Y. Heah, H. Yamagishi, K. Fujita, M. Sumitani, Y. Mikami, H. Yoshioka, Y. Oki and Y. Yamamoto, *Mater. Chem. Front.*, 2021, **5**, 5653–5657.

24 H.-Y. Liao, W. Y. Heah, Suharman, H. Yamagishi and Y. Yamamoto, *Chem. Lett.*, 2024, **53**, upae078.

25 T. Reynolds, N. Riesen, A. Meldrum, X. Fan, J. M. M. Hall, T. M. Monro and A. François, *Laser Photonics Rev.*, 2017, **11**, 1600265.

26 Z. Chen, J. Wu, Z. Song, Y. Zou, J. Hu, Y. Li, Y. Song, Y. Li, G. Bai, X. Li, Y. Zhu, X. Zhang, X. D. Wang, T. Song and B. Sun, *J. Phys. Chem. Lett.*, 2023, **14**, 8376–8384.

27 F. van Schoonhoven, Y. Tomishige, A. Abazi, A. Sánchez-Postigo, J. Chen, Y. Mikami, N. Tate, Y. Oki, C. Schuck and H. Yoshioka, *Opt. Mater. Express*, 2024, **14**, 1767.

28 A. Smirnov, A. Polushkin, A. Falchevskaya, M. Mikhailova, H. Shamkhi, L. Zelenkov, T. Pogosian, M. Morozov, S. Makarov and A. Vinogradov, *Adv. Opt. Mater.*, 2023, **11**, 2300385.

29 O. Oki, S. Kushida, A. Mikosch, K. Hatanaka, Y. Takeda, S. Minakata, J. Kuwabara, T. Kanbara, T. Dao, S. Ishii, T. Nagao, A. Kuehne, F. Deschler, R. Friend and Y. Yamamoto, *Mater. Chem. Front.*, 2018, **2**, 270–274.

30 R. A. Fletcher, J. A. Brazin, M. E. Staymates, B. A. Benner, Jr. and J. G. Gillen, *Talanta*, 2008, **76**, 949–955.

31 Y. Taniguchi, K. Nishimura, Y. Yoshida, S. Kim, L. Kamarulzaman, D. G. Priest and M. Ohno, *BioRxiv*, 2024, preprint, DOI: 10.1101/2024.12.05.625331.

32 A. N. Oraevsky, *Quantum Electron.*, 2002, **32**, 377–400.

33 H. Diab, C. Arnold, F. Lédée, G. Trippé-Allard, G. Delport, C. Vilar, F. Bretenaker, J. Barjon, J. S. Lauret, E. Deleporte and D. Garrot, *J. Phys. Chem. Lett.*, 2017, **8**, 2977–2983.

34 L. Wan, H. Chandrahalim, J. Zhou, Z. Li, C. Chen, S. Cho, H. Zhang, T. Mei, H. Tian, Y. Oki, N. Nishimura, X. Fan and L. J. Guo, *Opt. Express*, 2018, **26**, 5800.

35 F. Sedlmeir, R. Zeltner, G. Leuchs and H. G. Schwefel, *Opt. Express*, 2014, **22**, 30934–30942.